

Article

Functional Characterization of RNA Silencing Suppressor Encoded by Cotton Leafroll Dwarf Virus

Mary F. Akinyuwa  and Sung-Hwan Kang *

Department of Entomology and Plant Pathology, Auburn University, Auburn, AL 36849, USA; mfa0018@auburn.edu

* Correspondence: shk0015@auburn.edu; Tel.: +1-334-844-5006

Abstract: The P0 proteins encoded by Cotton leafroll dwarf virus (CLRDV) serve as viral suppressors of RNA silencing (VSR). CLRDV P0 proteins share a VSR-associated F-box-like motif. This study investigated the role of specific amino acid (aa) residues within the F-box-like motif, elucidating their implications for VSR potency, pathogenicity, and intracellular localization. Analysis of various single aa substitution mutants within the F-box-like motif to understand their effect on P0 proteins' VSR potency revealed that specific mutations significantly affect P0's ability to suppress RNA silencing, emphasizing the crucial role of the F-box-like motif. Subcellular localization examinations indicated that the P0 proteins associate with the nucleus and endoplasmic reticulum, which may be linked to their VSR function. Also, the induction of hypersensitive response (HR)-like symptoms and the accumulation of reactive oxygen species by P0 proteins was observed, suggesting their role as pathogenicity factors. These results indicated that specific mutations significantly affect the functions of multifaceted P0 proteins, highlighting the F-box-like motif's crucial role. Our study highlights the importance of further molecular investigations to elucidate how different CLRDV strains manifest various disease symptoms and severity. This is crucial considering the global economic importance of cotton and the potential emergence of more threatening CLRDV isolates.

Keywords: plant virus disease; cotton leafroll dwarf virus; *Polerovirus*; P0 protein; RNA silencing; pathogenicity



Citation: Akinyuwa, M.F.; Kang, S.-H. Functional Characterization of RNA Silencing Suppressor Encoded by Cotton Leafroll Dwarf Virus. *Agriculture* **2024**, *14*, 194. <https://doi.org/10.3390/agriculture14020194>

Academic Editor: Sayanta Bera

Received: 8 December 2023

Revised: 23 January 2024

Accepted: 25 January 2024

Published: 26 January 2024



Copyright: © 2024 by the authors. Licensee MDPI, Basel, Switzerland. This article is an open access article distributed under the terms and conditions of the Creative Commons Attribution (CC BY) license (<https://creativecommons.org/licenses/by/4.0/>).

1. Introduction

Cotton leafroll dwarf virus (CLRDV) is a newly emerging virus in the United States that has had a significant impact on cotton production in other countries [1–5]. CLRDV belongs to the family *Solemoviridae* and the genus *Polerovirus*, which consists of plant viruses expressing their proteins via a monopartite, positive-sense, single-stranded RNA genome comprising seven open reading frames (ORFs; Figure 1A) (reviewed in [6–11]). Among them, the P0 proteins encoded by ORF 0 have been extensively studied due to its pivotal role in countering the host's antiviral defense system, RNA silencing [12–17]. RNA silencing involves the recognition and subsequent degradation of viral double-stranded RNA [18–20]. Host factors participating in this process include an endonuclease called Dicer, responsible for generating siRNA, and the Argonaute (AGO) protein, which processes the target [21–23]. However, plant viruses have evolved their proteins to interfere with this process. In the case of the members of the genus *Polerovirus*, this interference is accomplished through the P0 proteins [12,14,15,17,24–29]. Consequently, the P0 protein is often associated with virus pathogenicity and symptom development [12,16,17,30–32]. Interestingly, despite being the most divergent ORF within the genome, P0 retains a conserved region referred to as the F-box-like motif in its N-terminal proximity (Figure 1B; [23,29,33–35]). In previous studies using mutant P0s with amino acid (aa) substitutions, this motif has been shown to be involved in VSR activity, intracellular location, and interactions with host proteins [15,22,23,28,31,36–39].

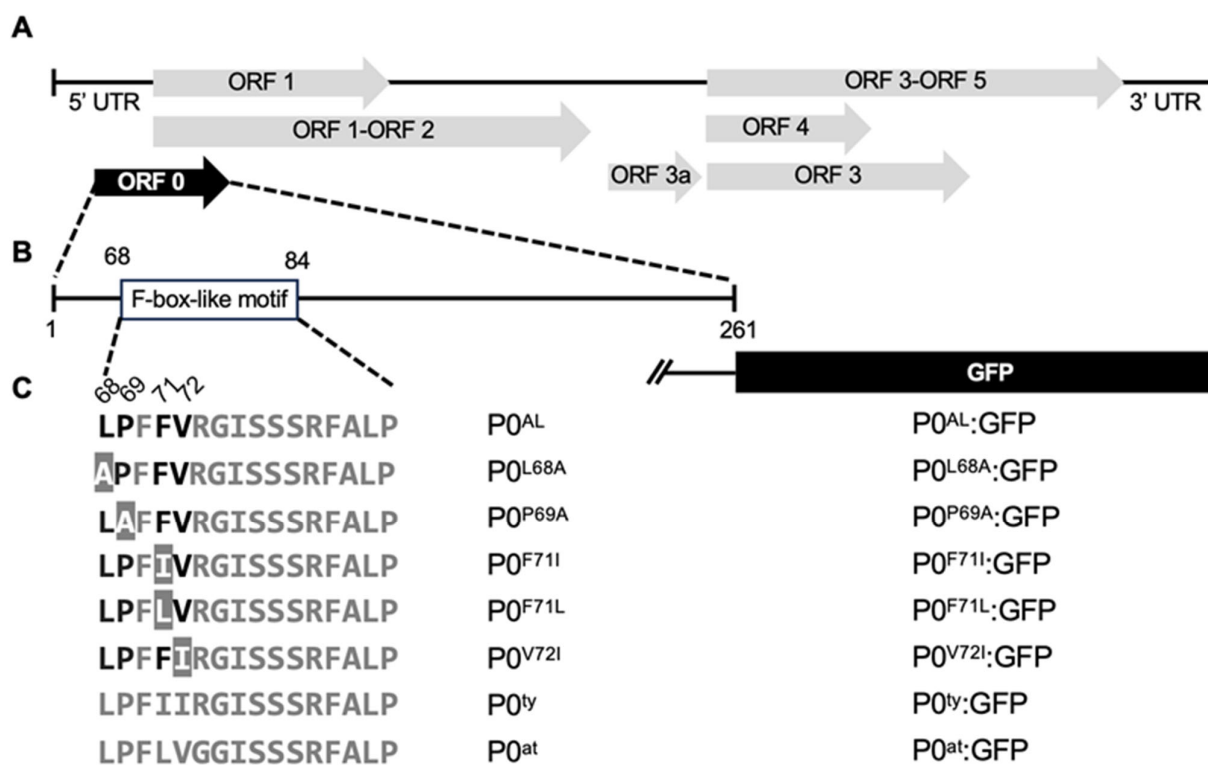


Figure 1. CLRVDV P0 cDNA constructs. (A) A schematic representation of the CLRVDV-AL genome. Open reading frames (ORFs) are represented as gray and black arrowhead boxes. UTR: untranslated region. (B) A schematic diagram of an F-box-like motif within the ORF 0. Amino acid (aa) residue positions corresponding to both ends of the motif are shown. (C) The aa substitutions within the F-box-like motif of CLRVDV P0 protein are identified as white letters on a gray background. Corresponding aa residue positions are shown. Another set of constructs with the same mutations fused with GFP ORF immediately after the 3' end of the P0 ORF (aa position 261) is depicted on the right.

Two previously reported CLRVDV strains, CLRVDV-ty and CLRVDV-at, exhibit variations in their pathogenicity levels and their ability to overcome resistance [1,12,14,40,41]. A study using an aa substitution that reverted a single aa within the F-box-like motif in CLRVDV-at to that found in CLRVDV-ty demonstrated an enhancement in its VSR potency and pathogenicity compared to the wild-type (WT) CLRVDV-at [1,12,14]. Similar changes in symptom development, VSR potency, intracellular localization, and viral pathogenicity resulting from aa substitution within the F-box-like motif were also reported in other members of the genus *Polerovirus* [15–17,29,31,42]. Interestingly, our recent study reported that cryptic pathogenicity displayed by a new strain of CLRVDV, recently isolated from the U.S. and designated as CLRVDV-AL [2,7], could be due to relatively weaker P0 protein activity as a VSR compared to other strains [24]. In that study, we discussed the three different aa residues within CLRVDV-AL's F-box-like motif compared to CLRVDV-ty and CLRVDV-at. However, it remained speculative, and the underlying function of this difference has not been demonstrated.

In this study, we aimed to identify specific aa residues associated with the characteristics of the P0 protein encoded by CLRVDV-AL (P0^{AL}). We generated a series of mutant P0 proteins with aa substitutions within the F-box-like motif using site-directed mutagenesis. Our study demonstrated how mutations or reversions within this motif could exert significant changes on the protein's VSR potency, intracellular localization, and pathogenicity. We also had a comprehensive discussion on the identified aa residues that were identified in comparison to other members of the genus *Polerovirus*. Our findings could provide insights into the emergence of potential new variants of CLRVDV, which could pose a significant threat to the cotton industry.

2. Materials and Methods

2.1. CLRDV P0 Constructs and Generation of P0^{AL} Mutant Constructs

The cDNA constructs of the ORF 0 from three different CLRDV strains (-ty, -at, and -AL) placed under the CaMV 35S promoter sequence in the binary plasmid pAIDEE (pAI-P0^{ty}, pAI-P0^{at}, and pAI-P0^{AL}, respectively) were previously described [24]. The cDNA constructs expressing a series of mutant P0^{AL}, which carry a single aa substitution mutation within the F-box-like motif, were constructed by Q5 site-directed mutagenesis kit (New England Biolabs, Ipswich, MA, USA). To generate pAI-P0^{L68A}, pAI-P0^{P69A}, and pAI-P0^{V72I}, pairs of oligomers were designed as per the manufacturer's protocol (Table 1) and used to amplify the cDNA encompassing the entire plasmid with the P0 sequence with the targeted mutation using the pGEMT-P0^{AL}, a cDNA of P0^{AL} coding sequence cloned into pGEM-T plasmid (Promega, Madison, WI, USA), as a template. The final products were verified by sequencing at Psomagen Inc. (Rockville, MD, USA) and amplified using a pair of oligomers, P0^{AL}.FW.ApaI and P0^{AL}.RV.XbaI (Table 1). The amplified product was purified using DNA Clean & Concentrator[®]-5 Kit (Zymo Research, Irvine, CA, USA), and subsequently digested using *ApaI* and *XbaI* restriction endonucleases (New England BioLabs, Ipswich, MA, USA) before being ligated with the binary plasmid pAIDEE (pAI; [43]) linearized with the same restriction endonucleases. Constructs were transformed into *E. coli* NEB[®] DH 5-alpha competent cells (New England Biolabs, Ipswich, MA, USA) and cells were screened on Luria–Bertani (LB) agar plates containing kanamycin (100 µg/µL). Final products were verified by sequencing at Psomagen Inc. (Rockville, MD, USA). The cDNA constructs expressing two mutants of P0^{AL} (pAI-P0^{F71I} and pAI-P0^{F71L}) were made using the cDNAs of ORF 0 prepared in a pUC57mini plasmid (Genscript, Piscataway, NJ, USA) with the corresponding site mutation. The synthesized products were digested with *KpnI* and *ApaI* restriction endonucleases (New England BioLabs, Ipswich, MA, USA). The excised fragments were purified using Zymoclean Gel DNA Recovery Kit (Zymo Research, Irvine, CA, USA), and ligated with the wild-type pAI-P0^{AL} linearized by the same restriction endonucleases using T4 DNA ligase (Promega, Madison, WI, USA). Constructs were transformed into *E. coli* NEB[®] DH 5-alpha competent cells and screened on LB agar plates containing kanamycin (100 µg/µL). Final products were verified by sequencing at Psomagen Inc. (Rockville, MD, USA).

Table 1. List of oligomers used for the generation of constructs and RT-qPCR assay.

Name	Sequence (5' to 3')	Tm *	References
Q-5 site-directed mutagenesis			
pAI-P0 ^{L68A} :FW	TCTTTTCTCGCTCCATTCTTCG	60.9	This study, Sections 2.2 and 2.3
pAI-P0 ^{L68A} :RV	AGAGAACGAAGGAGAAAAGA	54.3	
pAI-P0 ^{P69A} :FW	TTTTCTCCTTGCATTCTCGTTA	57.6	
pAI-P0 ^{P69A} :RV	AGAAGAGAACGAAGGAGAAA	54.3	
pAI-P0 ^{V72I} :FW	TCCATTCTTCATTAGGGGAATTT	57.6	
pAI-P0 ^{V72I} :RV	AGGAGAAAAAGAAGAGAACC	54.3	
Non-tagged P0s			
P0 ^{AL} .FW.ApaI	ACTAGGGCCCAACAATGTTGA ATTGATCATCTGC	73.1	This study, Section 2.2
P0 ^{AL} .RV.XbaI	GGACTCTAGATCAACTGCTTT CTCCTTCAC	70.8	
P0 ^{at} .FW.ApaI	ACTAGGGCCCAACAATGTTG AACTTGATTATCTGC	73.1	

Table 1. Cont.

Name	Sequence (5' to 3')	T _m *	References
GFP-tagged P0s			
P0:GFP-FW	TATGTGAAGGAGAAAAG CAGTATGGCTAGCAA AGGAGAAGA	76.0	This study, Section 2.3
P0:GFP-RV	TCTTCTCCTTTGCTAGCCA TACTGCTTCTCCTTCACATA	76.0	
GFP.RV.XbaI	<u>GTACTCTAGACTATT</u> TGTAGAGCTCATCC	67.4	
Sequence verification			
pAI SEQ FW	CCTCGAGAATTCTCAACACAAC	60.1	[24]
pAI SEQ RV	GCTCAACACATGAGCGAAACCC	64.2	
Quantitative mRNA analysis			
MFA.Gq-PCR:FW	GATGACGGGAAGTACAAGAC	58.4	[24]
MFA.Gq-PCR:RV	CGAGTACAACATAACTCACAC	58.4	
NbACTIN2-FW	CAATCCAGACACTGTACTTCTCTC	64.1	[44]
NbACTIN2-RV	AAGCTGCAGGTATCCATGAGACTA	63.6	

The amino acid substitution mutation-inducing nucleotides through Q-5 site-directed mutagenesis are indicated in bold characters. Restriction endonuclease (*XbaI* and *ApaI*) recognition sequences are italicized and underlined. The anticipated amplicon sizes are 3801 bp, 786 bp, 806 bp, and 1506 bp for Q-5 site-directed mutagenesis, non-tagged P0s, GFP-tagged P0s fragments, and GFP-tagged P0s overlap, respectively. * The unit for T_m is degrees Celsius.

2.2. Generation of the Green Fluorescent Protein-Tagged Constructs

To generate the green fluorescent protein (GFP)-tagged set of selected clones (pAI-P0^{ty}:GFP, and pAI-P0^{at}:GFP, pAI-P0^{AL}:GFP, and pAI-P0^{V72I}:GFP), overlap extension polymerase chain reaction (OE-PCR) was performed as previously described (Kang et al., 2018). The overlap was achieved by two PCR fragments with overhangs; one contains the 3' end of P0 with an extension into the 5' region of the GFP ORF, and the other contains the 5' end of GFP with an extension into P0 3'. The stop codon of the P0 was deleted to allow readthrough to the GFP ORF (Figure 1C). The first product, the P0-GFP fragment, was generated by fusing the 3' end of P0 or its mutants (P0^{V72I}:GFP) in front of the GFP ORF using PCR with a pair of oligomers, P0^{AL}.FW.*ApaI* and P0:GFP-RV (Table 1). For the P0^{at}:GFP fragment, a pair of oligomers, P0^{at}.FW.*ApaI* and P0:GFP-RV was used (Table 1). The full-length cDNA clones of GFP, P0^{AL}, P0^{V72I}, P0^{ty}, and P0^{at} placed under the CaMV 35S promoter sequence in the binary vector pAI were used to amplify the different fragments of the latter fragments (P0^{AL}:GFP, P0^{V72I}:GFP, P0^{ty}:GFP, and P0^{at}:GFP). The OE-PCR was performed to generate overlap fragments using two pairs of oligomers: P0^{AL}.FW.*ApaI* and GFP.RV.XbaI for P0^{AL}:GFP, P0^{V72I}:GFP, P0^{ty}:GFP, and P0^{at}.FW.*ApaI* and GFP.RV.XbaI for P0^{at}:GFP (Table 1). The overlap fragments were subsequently digested with *XbaI* and *ApaI* restriction endonucleases before ligating into the pAI plasmid. The remaining GFP-tagged P0 mutants (pAI-P0^{L68A}:GFP, pAI-P0^{P69A}:GFP, pAI-P0^{F71I}:GFP, and pAI-P0^{F71L}:GFP) were generated similarly as described above (See Section 2.2) except that pAI-P0^{AL}:GFP was used as a backbone for the ligation. Constructs were transformed into *E. coli* NEB[®] DH 5-alpha competent cells (Ipswich, MA, USA) and the transformants were screened on LB plates containing kanamycin (100 µg/µL). Final products were verified by sequencing at Psomagen Inc. (Rockville, MD, USA).

2.3. Agroinfiltration

Agroinfiltration of the constructs was conducted as previously described [45]. Briefly, *Agrobacterium tumefaciens* strain GV3101 was used for the transformation with the constructs described above. The cell suspensions were prepared at the optical density (OD_{600nm}) 1.0 or 0.5 with agroinfiltration buffer (10 mM MES, pH 5.85; 10 mM MgCl₂; 150 µM Acetosyringone), then infiltrated into the leaves of six-week-old *Nicotiana benthamiana* plants. The infiltrated plants were grown under 16 h/8 h of light/dark cycle.

2.4. Examination of Fluorescence in Plants

Six-week-old *N. benthamiana* 16c plants were co-infiltrated with equal volumes of *A. tumefaciens* cells containing pAI-P0^{AL}, pAI-P0^{ty}, pAI-P0^{at}, pAI-P0^{L68A}, pAI-P0^{P69A}, pAI-P0^{F71I}, pAI-P0^{F71L}, and pAI-P0^{V72I} or empty vector mixed with pAI-GFP. The expression of GFP transgene was examined using a hand-held UV (365 nm) lamp. For the quantitative analysis, the fluorescence intensity was calculated using the region of interest (ROI) on ImageJ v. 1.8.0 from fluorescence microscopy images. ROIs were strategically positioned within the microscopy images. For each microscopy image, pixel data were collected from five ROIs (each covering an area of 3,144,960 pixels), positioned at pre-determined locations (one in the middle and four near each corner). The data from each ROI included three values, excluding the highest and lowest, which were then averaged to obtain a representative value for the image.

2.5. Intracellular Localization

pAI-P0^{AL}:GFP, pAI-P0^{ty}:GFP, pAI-P0^{at}:GFP, pAI-P0^{L68A}:GFP, pAI-P0^{P69A}:GFP, pAI-P0^{F71I}:GFP, pAI-P0^{F71L}:GFP, and pAI-P0^{V72I}:GFP were infiltrated in *N. benthamiana* plants. Mesophyll cells of the leaves were observed at 5 dpi using an Echo Revolve fluorescence microscope (San Diego, CA, USA) with FITC cube (EX:470 ± 40 and EM:525 ± 50) and TxRED cube (EX:560 ± 40 and EM:630 ± 75) for the detection of GFP and RFP fluorescence, respectively. Images were captured using 20× objectives.

2.6. Relative Expression Levels of GFP mRNA

The relative expression levels of GFP mRNA were evaluated as previously described [24]. Briefly, 20 ng total RNA extracted using the RNeasy Plant Mini Kit (Qiagen, Hilden, Germany) was used as a template with specific pairs of oligomers as primers for RT-qPCR reactions in a total volume of 10 µL using the Luna[®] universal RT-qPCR system (New England Biolabs, Ipswich, MA, USA). Ct values were averaged for triplicates of each sample from three biological replicates using the $2^{-\Delta\Delta Ct}$ method [46].

2.7. Histochemical Staining

3,3'-diaminobenzidine (DAB) was used to detect reactive oxygen species (ROS) as previously described [47]. *N. benthamiana* leaves infiltrated as described in Section 2.4 at the optical density (OD_{600nm}) 0.5 were detached and washed three times with double-distilled water. Then, the leaves were incubated overnight in 1 mg/mL DAB-HCl (Sigma-Aldrich, St. Louis, MO, USA) prepared in boric acid buffer (50 mM, pH 7.6). The leaves were subsequently incubated in 95% ethanol with three changes before the images were taken. Relative DAB stain intensity was analyzed by measuring infiltrated patches' pixel intensity using regions of interest (ROIs) with ImageJ software v. 1.8.0 [48].

3. Results

3.1. A Single Amino Acid Substitution Enhances RNA Silencing Suppression Potency of CLRDV P0^{AL}

In our previous study [24], we reported that the P0 protein encoded by CLRDV-AL (P0^{AL}) acts as a weak VSR like the P0 protein of CLRDV-at (P0^{at}) and hypothesized its potential correlation with the cryptic traits of the virus during host infection. While P0^{AL} shares a conserved F-box-like motif with other CLRDV strains (Figure 1B), there are notable differences in specific aa residues when compared to CLRDV-ty and CLRDV-at [24]. We postulated that these residues might contribute to the distinctive characteristics of P0^{AL} and the cryptic traits of CLRDV-AL. To investigate this, we generated a series of constructs that express P0^{AL} mutants, each carrying a single aa substitution at specific residues within the F-box-like motif (Figure 1C; pAI-P0^{L68A}, pAI-P0^{P69A}, pAI-P0^{F71I}, pAI-P0^{F71L}, and pAI-P0^{V72I}), and compared their VSR potency to that of the WT P0^{AL} (Figure 2) by monitoring their ability to retain the fluorescence of GFP expressed in the leaves of *N. benthamiana* 16c plants that constitutively express GFP [49]. Each construct harboring the ORF of P0

from P0^{AL}, P0^{ty}, and the five mutants was co-infiltrated into the leaves of *N. benthamiana* 16C plants along with the pAI-GFP, which expresses a free GFP, via agroinfiltration. Upon observation under the UV light at 5 dpi, the non-infiltrated leaves showed a basal level of GFP fluorescence generated from their own GFP transgene expression (Figure 2A; Mock). However, leaves co-infiltrated with a free GFP construct and an empty vector did not exhibit GFP fluorescence and appeared purple due to chloroplast autofluorescence (Figure 2A; EV). As previously reported [12,24], more GFP fluorescence was observed in leaves co-infiltrated with P0^{ty}, while leaves co-infiltrated with P0^{AL} displayed less GFP fluorescence in the similar level shown by P0^{at} (Figure 2A; P0^{ty} and P0^{AL}). Among the P0^{AL} mutants, three (P0^{P69A}, P0^{F71I}, and P0^{F71L}) showed little to no GFP fluorescence, resembling the control infiltration using the empty vector. The green fluorescence in the leaves co-infiltrated with P0^{L68A} remained at a level similar to that observed with P0^{AL}. Notably, the leaves co-infiltrated with P0^{V72I} displayed strong GFP fluorescence, comparable to the level of green fluorescence observed in the leaves co-infiltrated with P0^{ty} (Figure 2A; V72I). The relative intensities of the GFP fluorescence, visually evaluated under UV light, indicated that the aa substitution at position 72 of P0^{AL} increased the VSR potency of P0^{AL} to a level similar to that of P0^{ty}.

To further evaluate the efficiency of RNA silencing suppression among the mutants, the patches of the infiltrated leaves were examined using a fluorescence microscope for quantitative analysis (Figure 2B, see Supplementary Figure S1 for more representative images). The relative fluorescence intensity was calculated and analyzed from more than 12 images per treatment using ImageJ (Figure 2C). The analysis revealed no significant difference in the GFP fluorescence within the infiltrated patches of three P0 mutants (P0^{P69A}, P0^{F71I}, and P0^{F71L}) compared to the control patch (EV) (Figure 2C; denoted as 'd'). Their green fluorescence levels were even lower than those analyzed from the buffer-infiltrated *N. benthamiana* 16c control (Figure 3C; 16c, denoted as 'c'), suggesting that these three mutant P0s failed to suppress RNA silencing. There was no significant difference in the green fluorescence levels between the patches infiltrated with P0^{L68A} and P0^{AL} (Figure 2C; denoted as 'b'), which is consistent with the results observed under the UV light (Figure 2A). The green fluorescence level of the patches infiltrated with P0^{V72I} was similar to that of P0^{ty}, and their fluorescence levels were significantly different ($p < 0.01$) than the other groups (Figure 2C; denoted as 'a'). To further validate our observation, the relative accumulation of GFP mRNA was analyzed by quantitative real-time PCR (Figure 2D). In line with the results in Figure 2C, the relative GFP mRNA levels were divided into three groups. The highest levels of GFP mRNA were detected in the tissue infiltrated with P0^{ty} or P0^{V72I}, aligning with the result shown in Figure 2C, where P0^{V72I} was denoted as a group 'a' along with P0^{ty}. Following this, P0^{AL} and P0^{L68A} formed an intermediate group, corresponding to the group 'b' in Figure 2C. The tissue infiltrated with P0^{P69A}, P0^{F71I}, or P0^{F71L} showed the lowest amount of GFP mRNA, similar to the control, EV. This aligns with the 'd' group, as noted in Figure 2C. These results collectively suggested that a single aa substitution, changing valine (V) to isoleucine (I) within the F-box-like motif, might have a role in the restoration of the VSR potency of P0^{AL} to a level comparable to that demonstrated by the P0 protein of CLR DV-ty.

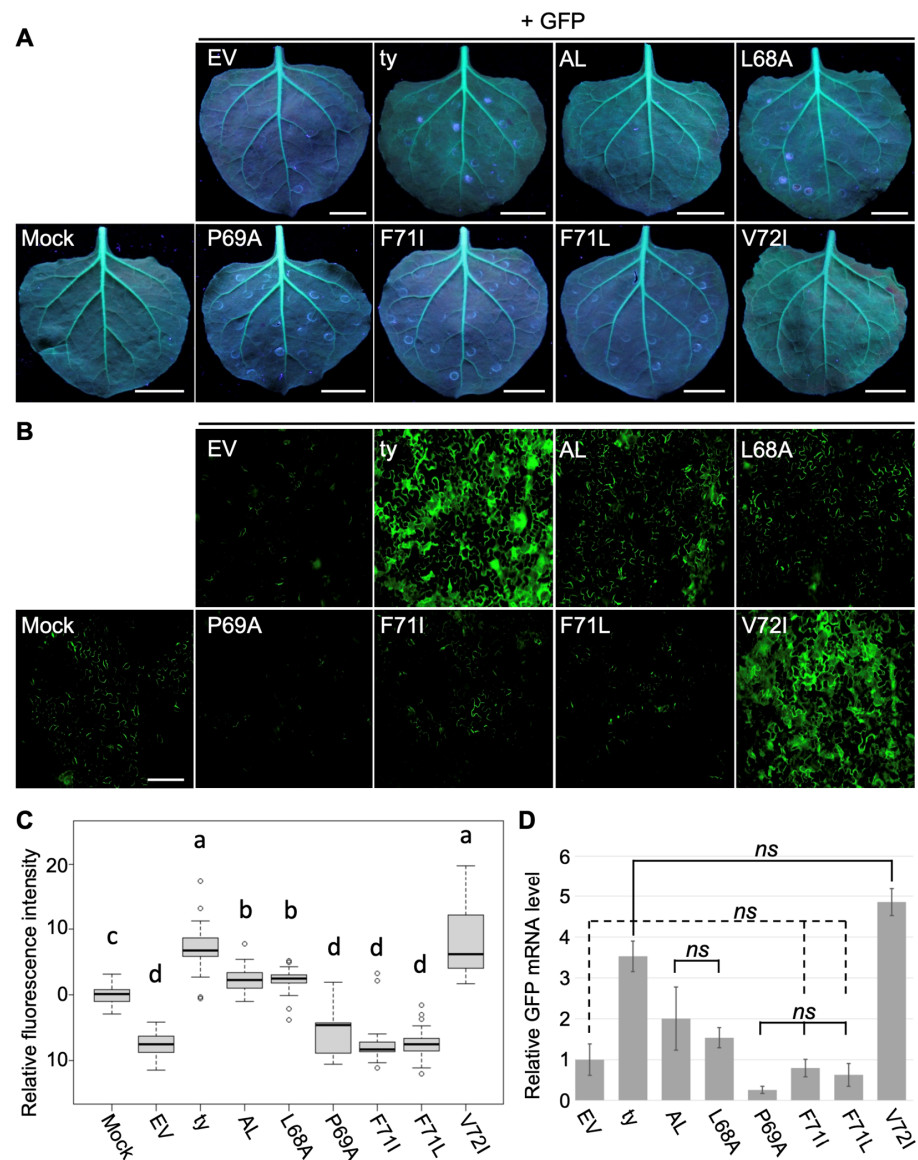


Figure 2. Comparison of VSR potency among CLRVDV P0s with single amino acid (aa) mutation within the F-box-like motif. RNA silencing suppression activity of the P0 proteins from CLRVDV-AL, CLRVDV-ty, and five CLRVDV-AL mutants (P0L68A, P0P69A, P0F71I, P0F71L, and P0V72I) were compared by co-expressing GFP and each P0 in GFP-transgenic *N. benthamiana* 16c plants via agroinfiltration. Images were taken at 5 dpi under the UV light ((A); scale bars = 2.5 cm) and using a fluorescence microscope ((B); scale bar = 180 μ m). Mock: non-infiltrated *N. benthamiana* 16c plant, EV: empty vector. All constructs were co-infiltrated with free GFP except 'Mock', as shown by the black line on the top of the panels. (C) The green fluorescence intensity was calculated using the ROI on ImageJ from more than 12 microscopy images per treatment. The relative intensity was analyzed by one-way ANOVA in R and depicted as a box and whisker plot. Each boxplot represents the interquartile range (middle 50% of the data), the lower and upper edges show the first and third quartile (25th and 75th percentile, respectively), and the median (horizontal line within the box). The whiskers are the contributions within the 1.5 interquartile range; open circles beyond these whiskers are considered outliers; significant differences, $p < 0.01$, were denoted by letters. (D) GFP mRNA levels in tissues co-infiltrated with a set shown in (A) were analyzed by RT-qPCR. Error bars indicate the standard deviation of the means of Ct values in three biological repeats using the actin2 reference gene and $2^{-\Delta\Delta Ct}$ method. Statistically significant differences were determined by Student's *t*-test. Non-significant groups are indicated (ns). Each non-significant group is significantly different from the other at $p < 0.01$, but not noted.

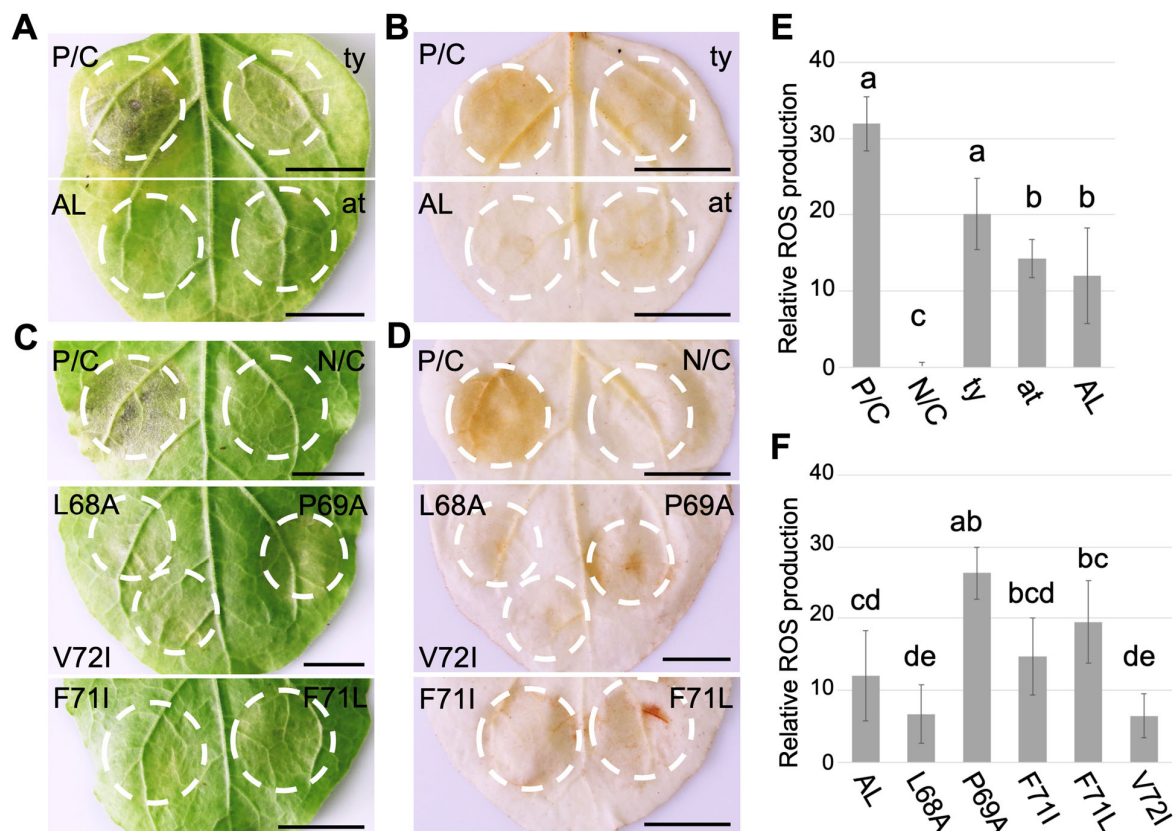


Figure 3. The P0 proteins of CLRDV and its mutants trigger an HR-like response and accumulate reactive oxygen species (ROS). The P0 proteins from three CLRDV strains (A,B) and the aa substitution mutants of P0AL (C,D) were transiently expressed in *Nicotiana benthamiana* via agroinfiltration. Left panels (A,C) are bright field images showing necrotic phenotype within the infiltrated patches (white dotted circle). Images were taken at 8 dpi. Scale bars = 2 cm. Middle panels (B,D) are infiltrated *N. benthamiana* leaves treated by 3,3'-diaminobenzidine (DAB) staining to demonstrate ROS accumulation within the infiltrated patches (white dotted circle). Images were taken at 3 dpi. P/C: P38 protein of Turnip crinkle virus, N/C: empty vector. Scale bars = 2 cm. Relative ROS production (E,F) was analyzed by measuring the color intensity of DAB staining using the ROI on ImageJ v. 1.8.0. Values are means from at least three independent patches per treatment. Error bars are standard deviation. Statistically significant differences, $p < 0.01$, determined by one-way ANOVA are denoted by letters.

3.2. F-Box-Like Motif Modulates HR-Like Response Triggered by CLRDV P0

Many poleroviral P0 proteins have been reported to induce hypersensitive response-like (HR-like) reactions, including the formation of necrotic lesions and the accumulation of reactive oxygen species (ROS) [17,30,32,50,51]. To determine if CLRDV P0 proteins elicit similar responses in plants, *N. benthamiana* leaves were infiltrated with the P0 constructs from three different strains (Figure 1C; pAI-P0^{AL}, pAI-P0^{at}, pAI-P0^{ty}) using agroinfiltration (Figure 3). Within 3 dpi, leaf patches expressing the P0 proteins began displaying HR-like necrotic lesions, which were observed up to 8 dpi (Figure 3A). However, the necrotic phenotype triggered by all three P0 proteins at 8 dpi was less severe than what was shown by the P38 protein of Turnip crinkle virus (P/C), a strong VSR shown to trigger a robust programmed cell death response [52]. Interestingly, among the three P0s, P0^{ty} induced a more pronounced necrotic lesion response than the P0 proteins from the atypical and AL strains. To investigate whether the cell death phenotype associated with the P0 proteins was also linked to ROS accumulation, we collected agroinfiltrated leaves at 3 dpi and subjected them to treatment with DAB to detect hydrogen peroxide (Figure 3B). The staining revealed

brown pigmentation in all constructs within the infiltrated patches (white dotted circles). Notably, the intensity of the brown pigmentation was visibly stronger in patches infiltrated with P0^{ty} or P/C compared to the patches infiltrated with P0^{at} or P0^{AL}. For a more precise assessment of the relative ROS production among these patches, we measured the intensity of the DAB staining (Figure 3E). The analysis indicated that P0^{ty} triggered a similar amount of ROS accumulation to that induced by P/C (Figure 3E; denoted as 'a'), which was higher than the accumulation resulting from P0^{AL} or P0^{at} (Figure 3E; denoted as 'b'). These results suggest that CLRVDV P0 proteins can induce HR-like responses and ROS accumulation, implying that P0 proteins may serve as pathogenicity factors. It is pertinent to note that the necrotic phenotype caused by the P0 proteins and their accompanied autofluorescence exhibited little interference with the microscopic GFP fluorescence analysis presented in Figure 2. The onset of the observed necrotic phenotype occurred after 7 dpi, whereas the fluorescence analysis was conducted at 5 dpi. Until 5 dpi, no noticeable autofluorescence was observed during the microscopic evaluation and image collection. Notably, P0^{P69A}, which induced the most pronounced necrotic phenotype (Figure 3F), exhibited the least GFP fluorescence (Figure 2D). While conversely, P0^{V72I}, which triggered minimal necrosis (Figure 3F), displayed the highest GFP fluorescence (Figure 2D).

A previous study on Pepper Vein Yellow Virus (PeVYV) demonstrated that aa substitutions within the F-box-like motif altered P0's capacity to induce an HR-like response and ROS accumulation [17]. To investigate whether the F-box-like motif within CLRVDV P0 proteins is similarly responsible for the phenotypes observed above, *N. benthamiana* leaves were infiltrated with the P0 constructs featuring five single aa substitutions as described above. The agroinfiltrated plants were maintained for up to 8 dpi (Figure 3C). Similar to what was observed with P0^{AL}, mild necrotic lesions were developed within the infiltrated patches expressing the mutant P0 proteins. Interestingly, more rapid lesion development was observed on the leaf patch infiltrated with P0^{P69A}. To determine the presence of accumulated ROS, we conducted DAB staining on the agroinfiltrated leaves collected at 3 dpi (Figure 3D). Upon visual examination, there appeared to be a subtle difference in the intensity of brown pigmentation among the P0 mutants. For more precise assessment, the relative ROS accumulation was analyzed using ImageJ (Figure 3F). As expected, the quantitative measurement revealed differences in ROS production among the mutant P0 proteins. Interestingly, two mutants, P0^{P68A} and P0^{V72I}, which demonstrated relatively higher VSR potency (Figure 2), accumulated a slightly lower amount of ROS than P0^{AL}. In contrast, three mutants, P0^{P69A}, P0^{F71I}, and P0^{F71L}, which exhibited little or no VSR potency (Figure 2), accumulated more ROS than P0^{AL}. These results suggest that aa residues within the F-box-like motif of the CLRVDV P0 protein play a role in its ability to induce ROS accumulation and HR-like lesions. Furthermore, the observed correlation between the phenotypes analyzed in Figures 2 and 3, particularly with respect to the same aa substitution mutations, highlights the significance of VSR potency for the P0 protein as a potential pathogenicity factor.

3.3. F-Box-Like Motif Plays a Role in the Intracellular Localization of CLRVDV P0

Understanding the intracellular localization of virus proteins provides insight to unravel their functions and roles in the viral infection cycle. The subcellular localization of polioviral P0 proteins has elucidated some key mechanisms of the P0 in viral infection [17,29]. To extend our understanding of CLRVDV-encoded P0 proteins, we examined the subcellular localization of the CLRVDV P0 protein by expressing it fused to the GFP ORF at its C-terminal end. The P0 proteins of three CLRVDV strains (Figure 1C; P0^{AL}:GFP, P0^{ty}:GFP, and P0^{at}:GFP) and aa substitution mutants of P0^{AL} (Figure 1C; P0^{L68A}:GFP, P0^{P69A}:GFP, P0^{F71I}:GFP, P0^{F71L}:GFP, and P0^{V72I}:GFP) were constructed and expressed in *N. benthamiana* plants via agroinfiltration along with a pAI:GFP (Figure 4). Upon the observation using a fluorescence microscope, the green fluorescence from pAI:GFP expressing a free GFP was evenly distributed along the cell membrane and within the nucleus (Figure 4A; panel GFP). However, when we examined the localization patterns of the green fluorescence

emitted by the GFP-fused P0 proteins from the three CLRDV strains, we observed marked differences as they exhibited irregular and intermittent green fluorescence distributed in the cytoplasm (Figure 4A; panels ty, at, and AL). Interestingly, we also noted a difference in the fluorescence pattern of P0^{AL}:GFP from P0^{ty}:GFP or P0^{at}:GFP. In contrast to P0^{ty}:GFP or P0^{at}:GFP, the green fluorescence from P0^{AL}:GFP was seen as multiple speckles that accumulated along the cell membrane (Figure 4A; AL, white triangles) and formed intense aggregates within the cytoplasm (Figure 4A; AL, red triangles). Furthermore, P0^{AL}:GFP did not display prominent nuclear fluorescence, which was observed in the case of P0^{ty}:GFP and P0^{at}:GFP (Figure 4A; ty and at, yellow triangles). In contrast to P0^{ty}:GFP or P0^{at}:GFP, which showed the green fluorescing nuclei in all observed cells, the nuclear fluorescence was observed in only 25% of the observed cells with P0^{AL}:GFP. Among the five mutants of P0^{AL} tagged with GFP, four of them exhibited a similar green fluorescence pattern to that of wild-type P0^{AL}:GFP. These mutants displayed large, intense aggregates within the cytoplasm and multiple speckles along the cell membrane, resembling the pattern observed with P0^{AL}:GFP (Figure 4A; L68A, P69A, F71I, and F71L). Conversely, P0^{V72I}:GFP displayed a different pattern. Its fluorescence was more akin to that of P0^{ty}:GFP or P0^{at}, characterized by pronounced nuclear fluorescence and fewer speckles along the cell membrane (Figure 4A; V72I, yellow triangles).

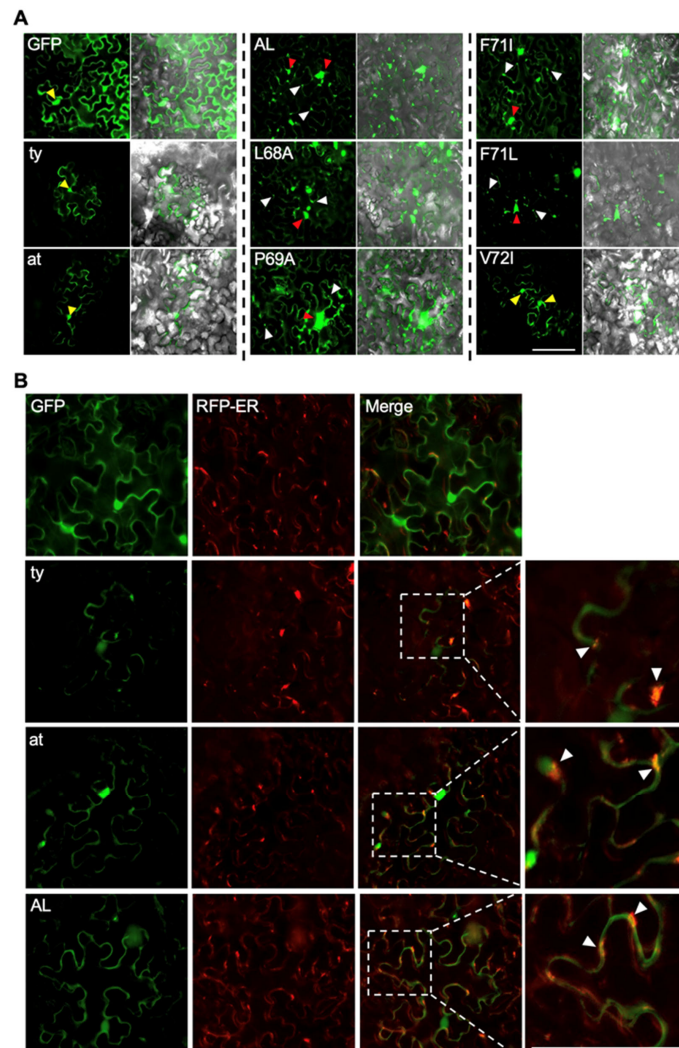


Figure 4. Subcellular localization of the P0 proteins. (A) The P0 proteins from three CLRDV strains (ty, at, and AL) and the amino acid (aa) substitution mutants of P0AL (L68A, P69A, F71I, F71L, and V72I)

fused to the green fluorescent protein (GFP) were transiently expressed in *Nicotiana benthamiana* leaves via agroinfiltration. Each set of images consists of two panels showing the GFP channel (left) and the GFP channel merged with the trans channel (right). Yellow, red, and white triangles point to nuclei, aggregates, and speckles, respectively. (B) The P0 proteins from three CLRVDV strains (ty, at, and AL) fused to GFP were transiently expressed in *N. benthamiana* via agroinfiltration along with the red fluorescent protein (RFP)-tagged endoplasmic reticulum (ER) cellular marker (RFP-ER). Zoomed-in images on the far-right column correspond to the dotted square in the 'Merge' panels. White triangles point to the co-localized fluorescent molecules. Representative images were shown from four independent agroinfiltration sets for (A,B) panels. Images were taken at 5 dpi. Scale bars = 100 μ m.

The intriguing subcellular localization patterns observed for CLRVDV P0 proteins, characterized by multiple speckles and aggregates, prompted us to investigate the mechanisms underlying their function as VSR. Previous studies have revealed that the subcellular localization of poleroviral P0 proteins can influence their role in the degradation of AGO proteins when they are excluded from the endoplasmic reticulum (ER) membrane [38,53]. To explore this further with CLRVDV P0s, we conducted a similar approach by co-expressing GFP-fused P0 proteins from the three CLRVDV strains (ty, at, and AL) along with a red fluorescent protein-tagged ER marker (RFP-ER; [54]), then observed the fluorescence in two different channels using a fluorescence microscope (Figure 4B). In the cells displaying both green and red fluorescence, indicating the co-expression of two infiltrated plasmid constructs, several bright orange spots were observed (Figure 4B; white triangles). These spots were not readily found in the leaves co-infiltrated with RFP-ER and a free GFP construct, implying that GFP was targeted to ER when fused to CLRVDV P0s. These results align with previous studies that investigated other members of the genus *Polerovirus*, suggesting that CLRVDV P0 proteins suppress RNA silencing through their association with the ER membrane, where they possibly interact with the host proteins to facilitate the degradation of AGO proteins.

4. Discussion

In this study, we examined the properties of the F-box-like motif present in the suppressor of RNA silencing encoded by a newly isolated cotton-infecting *Polerovirus*, CLRVDV-AL. We achieved this by using a series of mutant proteins with single aa substitutions. These aa substitutions were selected based on the variation found among three different strains of CLRVDV [24]. Through the five P0 mutants (P0^{L68A}, P0^{P69A}, P0^{F71I}, P0^{F71L}, and P0^{V72I}), we demonstrated how a single aa modification within the F-box-like motif could lead to alterations in the protein's function.

The leucine (L) at the aa position 68 is conserved among CLRVDVs and most members in the genus *Polerovirus*. In our study, P0^{L68A}, substituting this L with alanine (A), showed minimal impact on the overall VSR potency (Figure 2). While it might imply an insignificant contribution of this residue to the mechanism of RNA silencing suppression by the P0 protein, it is important to consider that the ineffectiveness of substituting L with A could be attributed to the structural and chemical similarity between the two amino acids. In contrast, the substitution of Proline (P) at the aa position 69 to A (P0^{P69A}) resulted in a complete loss of VSR potency (Figure 2). This can be attributed to the importance of P for maintaining the structural integrity and stability of the protein, as noted in previous studies [55,56]. A similar loss of VSR potency induced by the change in these two aa residues was also reported from the P0 proteins of Maize yellow dwarf virus-RMV2 [29], Potato leafroll virus [42], and PeVYV [17]. A more notable case relates to the substitution at the aa position 72, converting V to I. Isoleucine is the aa present in P0^{ty}, a stronger VSR among three CLRVDVs [24]. Remarkably, P0^{V72I} demonstrated a robust silencing suppression potency similar to that of P0^{ty}. This suggests that a naturally occurring mutation at this residue during viral replication in the field could give rise to a variant with increased VSR potency, potentially causing more severe disease [57,58]. It is noteworthy, and also concerning, that a variant carrying such substitution at this residue has recently been isolated in Texas,

resulting in severe symptoms in the host [58]. However, the enhancement in VSR potency appears to depend on the other residues within the F-box-like motif as well. A prior study involving P0 proteins from CLRDV-ty and CLRDV-at conducted by Agrofoglio et al. [12] introduced the same mutation on the aa position 72 and compared the VSR potency. In that study, a change from V to I on P0^{at} enhanced the VSR potency. However, it was a slight increase, unlike what was shown by P0^{AL} carrying the same substitution (P0^{V72I}) here, suggesting that other residues within the motif may also influence and collaborate in determining the overall VSR function of the P0 protein. Our results from two other mutants, P0^{F71I} and P0^{F71L}, which exhibited little to no suppression activity, further support the hypothesis that the VSR potency of the P0 protein is not solely determined by a single aa at position 72.

A previous study that delved into the function of aa residues within the F-box-like motif of PeVYV P0 revealed that a specific aa, leucine, positioned at the start of the motif, played a critical role in inducing programmed cell death when expressed in the host [32]. This is the same leucine found at the aa position 68 in P0^{AL} (Figure 1C). Our results align with it, as we observed a reduction in the formation of HR-like lesions and the accumulation of ROS by P0^{L68A} (Figure 3). However, in our study, which involved more mutants targeting additional aa residues, P0^{V72I} induced less necrosis, much like P0^{L68A}. On the contrary, the necrosis triggered by three mutants (P0^{P69A}, P0^{F71I}, and P0^{F71L}) that exhibited little to no VSR activity was more severe compared to P0^{AL} and approached the levels induced by P0^{ty} or P0^{at}. It is important to note that it is yet premature to draw any conclusions regarding a direct correlation between the functions of specific residues within the F-box-like motif in suppressing RNA silencing and inducing an HR-like response. To answer this, further investigations, such as comprehensive surveys involving multiple residue substitution mutants or examinations of the interactions between the P0 protein and host proteins involved in the RNA silencing pathway, will be needed to gain a deeper understanding of these mechanisms.

The mechanism of RNA silencing suppression by the P0 protein has been extensively explored in other members of the genus *Polerovirus*. In these studies, it has been shown that P0 proteins effectively seize a host factor, SKP1, to degrade AGO proteins [33,38,59]. Notably, in two poleroviruses, Beet western yellows virus (BWYV) and Turnip yellows virus (TuYV), it has been demonstrated that their P0 proteins interact with ER membrane-bound AGO1 and subsequently form vesicles [38,53]. Additionally, BWYV P0 triggers the removal of unloaded AGO1 from the nucleus [59], while TuYV P0 degrades AGO4, which predominantly localizes in the soluble fraction [53,60]. Our results, as shown in Figure 4B, indicate that the P0 proteins from three different CLRDV strains share an association with the ER, suggesting a conserved mechanism of RNA silencing suppression common to them, irrespective of the strain. However, it is important to note that the prominent nuclear accumulation observed in P0^{ty}, P0^{at}, and P0^{V72I} (Figure 4A) implies that nuclear localization may have contributed to differentiating their VSR potency, potentially making them more effective than P0^{AL} and the other P0^{AL} mutants.

5. Conclusions

It is evident from our results that the collective variation within the F-box-like motif of the P0 proteins among the three strains of CLRDV contributes to the difference in the levels of silencing suppression potency and pathogenicity. However, it is unclear if there is a correlation between VSR potency and subcellular localization, and whether this leads to the altered pathogenicity of the virus. CLRDV, as an RNA virus, is prone to frequent mutations and the potential emergence of new isolates that can cause more severe disease in cotton. Given the global economic significance of cotton, it is imperative to elucidate the pathogenicity mechanism of CLRDV through further molecular investigations of the P0 protein and the host factors involved with it. This will help us understand the range of disease symptoms and severity caused by different CLRDV strains.

Supplementary Materials: The following supporting information can be downloaded at: <https://www.mdpi.com/article/10.3390/agriculture14020194/s1>, Figure S1: Fluorescence microscopy images.

Author Contributions: M.F.A.: Methodology, formal analysis, investigation, validation, visualization, and writing an original draft. S.-H.K.: Conceptualization, funding acquisition, methodology, validation, resources, supervision, review, and editing. All authors have read and agreed to the published version of the manuscript.

Funding: This research was supported by the Alabama Agricultural Experiment Station and the Hatch program of the National Institute of Food and Agriculture, U.S. Department of Agriculture (ALA015-1-19124), and Cotton Inc. (#23-569AL).

Institutional Review Board Statement: Not applicable.

Data Availability Statement: The data used to support the conclusions of this article will be made available upon request. Further inquiries can be directed to the corresponding author.

Acknowledgments: The authors would like to thank Feng Qu at the Ohio State University for providing pAIDEE (pAI) and RFP-ER plasmids used in this study. The findings and conclusions in this article have not been formally disseminated by the U.S. Department of Agriculture and should not be construed to represent any agency determination or policy.

Conflicts of Interest: The authors declare no conflicts of interest.

References

1. Agrofoglio, Y.C.; Delfosse, V.C.; Casse, M.F.; Hopp, H.E.; Kresic, I.B.; Distéfano, A.J. Identification of a New Cotton Disease Caused by an Atypical Cotton Leafroll Dwarf Virus in Argentina. *Phytopathology* **2017**, *107*, 369–376. [[CrossRef](#)]
2. Avelar, S.; Schrimsher, D.W.; Lawrence, K.S.; Brown, J.K. First Report of Cotton leafroll dwarf virus Associated with Cotton Blue Disease Symptoms in Alabama. *Plant Dis.* **2019**, *103*, 592. [[CrossRef](#)]
3. Bag, S.; Roberts, P.M.; Kemerait, R.C. Cotton Leafroll Dwarf Disease: An Emerging Virus Disease on Cotton in the U.S. *Crop. Soils* **2021**, *54*, 18–22. [[CrossRef](#)]
4. Distéfano, A.J.; Kresic, I.B.; Hopp, H.E. The complete genome sequence of a virus associated with cotton blue disease, cotton leafroll dwarf virus, confirms that it is a new member of the genus Polerovirus. *Arch. Virol.* **2010**, *155*, 1849–1854. [[CrossRef](#)]
5. Edula, S.R.; Bag, S.; Milner, H.; Kumar, M.; Suassuna, N.D.; Chee, P.W.; Kemerait, R.C.; Hand, L.C.; Snider, J.L.; Srinivasan, R.; et al. Cotton leafroll dwarf disease: An enigmatic viral disease in cotton. *Mol. Plant Pathol.* **2023**, *24*, 513–526. [[CrossRef](#)]
6. Delfosse, V.C.; Barón, M.P.B.; Distéfano, A.J. What we know about poleroviruses: Advances in understanding the functions of polerovirus proteins. *Plant Pathol.* **2021**, *70*, 1047–1061. [[CrossRef](#)]
7. Avelar, S.; Ramos-Sobrinho, R.; Conner, K.; Nichols, R.L.; Lawrence, K.S.; Brown, J.K. Characterization of the Complete Genome and P0 Protein for a Previously Unreported Genotype of Cotton Leafroll Dwarf Virus, an Introduced Polerovirus in the United States. *Plant Dis.* **2020**, *104*, 780–786. [[CrossRef](#)] [[PubMed](#)]
8. Corrêa, R.L.; Silva, T.F.; Simões-Araújo, J.L.; Barroso, P.A.V.; Vidal, M.S.; Vaslin, M.F.S. Molecular characterization of a virus from the family *Luteoviridae* associated with cotton blue disease. *Arch. Virol.* **2005**, *150*, 1357–1367. [[CrossRef](#)] [[PubMed](#)]
9. King, A.M.Q.; Adams, M.J.; Carstens, E.B.; Lefkowitz, E.J. (Eds.) Family-Luteoviridae. In *Virus Taxonomy*; Elsevier: San Diego, CA, USA, 2012; pp. 1045–1053. [[CrossRef](#)]
10. Smirnova, E.; Firth, A.E.; Miller, W.A.; Scheidecker, D.; Brault, V.; Reinbold, C.; Rakotondrafara, A.M.; Chung, B.Y.-W.; Ziegler-Graff, V. Discovery of a Small Non-AUG-Initiated ORF in Poleroviruses and Luteoviruses That Is Required for Long-Distance Movement. *PLoS Pathog.* **2015**, *11*, e1004868. [[CrossRef](#)] [[PubMed](#)]
11. Sömera, M.; Fargette, D.; Hébrard, E.; Sarmiento, C. ICTV virus taxonomy profile: Solemoviridae 2021. *J. Gen. Virol.* **2021**, *102*, 001707. [[CrossRef](#)]
12. Agrofoglio, Y.C.; Delfosse, V.C.; Casse, M.F.; Hopp, H.E.; Kresic, I.B.; Ziegler-Graff, V.; Distéfano, A.J. P0 protein of cotton leafroll dwarf virus-atypical isolate is a weak RNA silencing suppressor and the avirulence determinant that breaks the cotton *Cbd* gene-based resistance. *Plant Pathol.* **2019**, *68*, 1059–1071. [[CrossRef](#)]
13. Almasi, R.; Miller, W.A.; Ziegler-Graff, V. Mild and severe cereal yellow dwarf viruses differ in silencing suppressor efficiency of the P0 protein. *Virus Res.* **2015**, *208*, 199–206. [[CrossRef](#)]
14. Delfosse, V.C.; Agrofoglio, Y.C.; Casse, M.F.; Kresic, I.B.; Hopp, H.E.; Ziegler-Graff, V.; Distéfano, A.J. The P0 protein encoded by cotton leafroll dwarf virus (CLRDV) inhibits local but not systemic RNA silencing. *Virus Res.* **2014**, *180*, 70–75. [[CrossRef](#)] [[PubMed](#)]
15. Sun, Q.; Zhuo, T.; Zhao, T.Y.; Zhou, C.J.; Li, Y.Y.; Wang, Y.; Li, D.W.; Yu, J.L.; Han, C.G. Functional Characterization of RNA Silencing Suppressor P0 from Pea Mild Chlorosis Virus. *Int. J. Mol. Sci.* **2020**, *21*, 7136. [[CrossRef](#)] [[PubMed](#)]
16. Wang, K.-D.; Dughbaj, M.A.; Nguyen, T.T.V.; Nguyen, T.Q.Y.; Oza, S.; Valdez, K.; Anda, P.; Waltz, J.; Sacco, M.A. Systematic mutagenesis of Polerovirus protein P0 reveals distinct and overlapping amino acid functions in *Nicotiana glutinosa*. *Virology* **2023**, *578*, 24–34. [[CrossRef](#)]

17. Wang, L.; Tian, P.; Yang, X.; Zhou, X.; Zhang, S.; Li, C.; Yang, X.; Liu, Y. Key Amino Acids for Pepper Vein Yellows Virus P0 Protein Pathogenicity, Gene Silencing, and Subcellular Localization. *Front. Microbiol.* **2021**, *12*, 1653. [[CrossRef](#)] [[PubMed](#)]
18. Hammond, S.M. Dicing and slicing: The core machinery of the RNA interference pathway. *FEBS Lett.* **2005**, *579*, 5822–5829. [[CrossRef](#)]
19. Li, F.; Wang, A. RNA-Targeted Antiviral Immunity: More Than Just RNA Silencing. *Trends Microbiol.* **2019**, *27*, 792–805. [[CrossRef](#)]
20. Voinnet, O. Induction and suppression of RNA silencing: Insights from viral infections. *Nat. Rev. Genet.* **2005**, *6*, 206–220. [[CrossRef](#)]
21. Blevins, T.; Rajeswaran, R.; Shivaprasad, P.V.; Beknazariants, D.; Si-Ammour, A.; Park, H.-S.; Vazquez, F.; Robertson, D.; Meins, F.; Hohn, T.; et al. Four plant Dicers mediate viral small RNA biogenesis and DNA virus induced silencing. *Nucleic Acids Res.* **2006**, *34*, 6233–6246. [[CrossRef](#)]
22. Derrien, B.; Clavel, M.; Baumberger, N.; Iki, T.; Sarazin, A.; Hacquard, T.; Ponce, M.R.; Ziegler-Graff, V.; Vaucheret, H.; Micol, J.L.; et al. A Suppressor Screen for AGO1 Degradation by the Viral F-Box P0 Protein Uncovers a Role for AGO DUF1785 in sRNA Duplex Unwinding. *Plant Cell* **2018**, *30*, 1353–1374. [[CrossRef](#)]
23. Pazhouhandeh, M.; Dieterle, M.; Marrocco, K.; Lechner, E.; Berry, B.; Brault, V.; Hemmer, O.; Kretsch, T.; Richards, K.E.; Genschik, P.; et al. F-box-like domain in the polerovirus protein P0 is required for silencing suppressor function. *Proc. Natl. Acad. Sci. USA* **2006**, *103*, 1994–1999. [[CrossRef](#)]
24. Akinyuwa, M.F.; Price, B.K.; Martin, K.M.; Kang, S.-H. A newly isolated cotton-infecting Polerovirus with cryptic pathogenicity encodes a weak suppressor of RNA silencing. *Front. Agron.* **2023**, *5*, 123516. [[CrossRef](#)]
25. Bortolamiol-Bécet, D.; Monsion, B.; Chapuis, S.; Hleibieh, K.; Scheidecker, D.; Alioua, A.; Bogaert, F.; Revers, F.; Brault, V.; Ziegler-Graff, V. Phloem-Triggered Virus-Induced Gene Silencing Using a Recombinant Polerovirus. *Front. Microbiol.* **2018**, *9*, 2449. [[CrossRef](#)]
26. Fusaro, A.F.; Correa, R.L.; Nakasugi, K.; Jackson, C.; Kawchuk, L.; Vaslin, M.F.S.; Waterhouse, P.M. The Enamovirus P0 protein is a silencing suppressor which inhibits local and systemic RNA silencing through AGO1 degradation. *Virology* **2012**, *426*, 178–187. [[CrossRef](#)]
27. Kozłowska-Makulska, A.; Guilley, H.; Szyndel, M.S.; Beuve, M.; Lemaire, O.; Herrbach, E.; Bouzoubaa, S. P0 proteins of European beet-infecting poleroviruses display variable RNA silencing suppression activity. *J. Gen. Virol.* **2010**, *91*, 1082–1091. [[CrossRef](#)]
28. Li, Y.; Sun, Q.; Zhao, T.; Xiang, H.; Zhang, X.; Wu, Z.; Zhou, C.; Zhang, X.; Wang, Y.; Zhang, Y.; et al. Interaction between Brassica yellows virus silencing suppressor P0 and plant SKP1 facilitates stability of P0 in vivo against degradation by proteasome and autophagy pathways. *New Phytol.* **2019**, *222*, 1458–1473. [[CrossRef](#)] [[PubMed](#)]
29. Wang, F.; Zhao, X.; Dong, Q.; Zhou, B.L.; Gao, Z.L. Characterization of an RNA silencing suppressor encoded by maize yellow dwarf virus-RMV2. *Virus Genes* **2018**, *54*, 570–577. [[CrossRef](#)] [[PubMed](#)]
30. Liang, K.-L.; Liu, J.-Y.; Bao, Y.-Y.; Wang, Z.-Y.; Xu, X.-B. Screening and Identification of Host Factors Interacting with the Virulence Factor P0 Encoded by Sugarcane Yellow Leaf Virus by Yeast Two-Hybrid Assay. *Genes* **2023**, *14*, 1397. [[CrossRef](#)]
31. Rashid, M.-O.; Zhang, X.-Y.; Wang, Y.; Li, D.-W.; Yu, J.-L.; Han, C.-G. The Three Essential Motifs in P0 for Suppression of RNA Silencing Activity of *Potato leafroll virus* Are Required for Virus Systemic Infection. *Viruses* **2019**, *11*, 170. [[CrossRef](#)]
32. Wang, K.; Empleo, R.; Nguyen, T.T.V.; Moffett, P.; Sacco, M.A. Elicitation of hypersensitive responses in *Nicotiana glutinosa* by the suppressor of RNA silencing protein P0 from poleroviruses. *Mol. Plant Pathol.* **2016**, *16*, 435–448. [[CrossRef](#)]
33. Baumberger, N.; Tsai, C.-H.; Lie, M.; Havecker, E.; Baulcombe, D.C. The Polerovirus Silencing Suppressor P0 Targets ARGONAUTE Proteins for Degradation. *Curr. Biol.* **2007**, *17*, 1609–1614. [[CrossRef](#)]
34. Cascardo, R.-S.; Arantes I.-L.; Silva T.-F.; Sachetto-Martins G.; Vaslin M.-F.; Corrêa R.-L. Function and diversity of P0 proteins among cotton leafroll dwarf virus isolates. *Virol J.* **2015**, *12*, 123. [[CrossRef](#)]
35. LaTourrette, K.; Holste, N.M.; Garcia-Ruiz, H. Polerovirus genomic variation. *Virus Evol.* **2021**, *7*, veab102. [[CrossRef](#)]
36. Bortolamiol, D.; Pazhouhandeh, M.; Marrocco, K.; Genschik, P.; Ziegler-Graff, V. The Polerovirus F Box Protein P0 Targets ARGONAUTE1 to Suppress RNA Silencing. *Curr. Biol.* **2007**, *17*, 1615–1621. [[CrossRef](#)]
37. Correa, R.L.; Bruckner, F.P.; Cascardo, R.D.S.; Alfenas-Zerbini, P. The Role of F-Box Proteins during Viral Infection. *Int. J. Mol. Sci.* **2013**, *14*, 4030–4049. [[CrossRef](#)] [[PubMed](#)]
38. Derrien, B.; Baumberger, N.; Schepetilnikov, M.; Viotti, C.; De Cillia, J.; Ziegler-Graff, V.; Isono, E.; Schumacher, K.; Genschik, P. Degradation of the antiviral component ARGONAUTE1 by the autophagy pathway. *Proc. Natl. Acad. Sci. USA* **2012**, *109*, 15942–15946. [[CrossRef](#)]
39. Sun, Q.; Li, Y.-Y.; Wang, Y.; Zhao, H.-H.; Zhao, T.-Y.; Zhang, Z.-Y.; Li, D.-W.; Yu, J.-L.; Wang, X.-B.; Zhang, Y.-L.; et al. Brassica yellows virus P0 protein impairs the antiviral activity of NbRAF2 in *Nicotiana benthamiana*. *J. Exp. Bot.* **2018**, *69*, 3127–3139. [[CrossRef](#)] [[PubMed](#)]
40. Da Silva, A.K.F.; Romanel, E.; Silva, T.D.F.; Castilhos, Y.; Schrago, C.G.; Galbieri, R.; Bélot, J.-L.; Vaslin, M.F.S. Complete genome sequences of two new virus isolates associated with cotton blue disease resistance breaking in Brazil. *Arch. Virol.* **2015**, *160*, 1371–1374. [[CrossRef](#)]
41. Galbieri, R.; Boldt, A.S.; Scoz, L.B.; Rodrigues, S.M.; Rabel, D.O.; Belot, J.L.; Vaslin, M.; Silva, T.d.F.; Kobayashi, L.; Chitarra, L.G. Cotton blue disease in central-west Brazil: Occurrence, vector (*Aphis gossypii*) control levels and cultivar reaction. *Trop. Plant Pathol.* **2017**, *42*, 468–474. [[CrossRef](#)]

42. Zhuo, T.; Li, Y.-Y.; Xiang, H.-Y.; Wu, Z.-Y.; Wang, X.-B.; Wang, Y.; Zhang, Y.-L.; Li, D.-W.; Yu, J.-L.; Han, C.-G. Amino Acid Sequence Motifs Essential for P0-Mediated Suppression of RNA Silencing in an Isolate of *Potato leafroll virus* from Inner Mongolia. *Mol. Plant-Microbe Interact.* **2014**, *27*, 515–527. [[CrossRef](#)]
43. Lin, J.; Guo, J.; Finer, J.; Dorrance, A.E.; Redinbaugh, M.G.; Qu, F. The Bean Pod Mottle Virus RNA2-Encoded 58-Kilodalton Protein P58 Is Required in *cis* for RNA2 Accumulation. *J. Virol.* **2014**, *88*, 3213–3222. [[CrossRef](#)]
44. Luo, C.; Wang, Z.Q.; Liu, X.; Zhao, L.; Zhou, X.; Xie, Y. Identification and Analysis of Potential Genes Regulated by an Alphasatellite (TYLCCNA) that Contribute to Host Resistance against Tomato Yellow Leaf Curl China Virus and Its Betasatellite (TYLCCNV/TYLCCNB) Infection in *Nicotiana benthamiana*. *Viruses* **2019**, *11*, 442. [[CrossRef](#)]
45. Kang, S.-H.; Bak, A.; Kim, O.-K.; Folimonova, S.Y. Membrane association of a nonconserved viral protein confers virus ability to extend its host range. *Virology* **2015**, *482*, 208–217. [[CrossRef](#)]
46. Livak, K.J.; Schmittgen, T.D. Analysis of relative gene expression data using real-time quantitative PCR and the $2^{-\Delta\Delta CT}$ Method. *Methods* **2001**, *25*, 402–408. [[CrossRef](#)]
47. Kang, S.-H.; Sun, Y.-D.; Atallah, O.O.; Huguet-Tapia, J.C.; Noble, J.D.; Folimonova, S.Y. A Long Non-Coding RNA of *Citrus tristeza virus*: Role in the Virus Interplay with the Host Immunity. *Viruses* **2019**, *11*, 436. [[CrossRef](#)]
48. Schindelin, J.; Arganda-Carreras, I.; Frise, E.; Kaynig, V.; Longair, M.; Pietzsch, T.; Preibisch, S.; Rueden, C.; Saalfeld, S.; Schmid, B.; et al. Fiji: An open-source platform for biological-image analysis. *Nat. Methods* **2012**, *9*, 676–682. [[CrossRef](#)] [[PubMed](#)]
49. Ruiz, M.T.; Voignet, O.; Baulcombe, D.C. Initiation and Maintenance of Virus-Induced Gene Silencing. *Plant Cell* **1998**, *10*, 937–946. [[CrossRef](#)] [[PubMed](#)]
50. Mangwende, T.; Wang, M.-L.; Borth, W.; Hu, J.; Moore, P.H.; Mirkov, T.E.; Albert, H.H. The P0 gene of Sugarcane yellow leaf virus encodes an RNA silencing suppressor with unique activities. *Virology* **2009**, *384*, 38–50. [[CrossRef](#)] [[PubMed](#)]
51. Zhang, X.-Y.; Li, Y.-Y.; Wang, Y.; Li, D.-W.; Yu, J.-L.; Han, C.-G. Comparative Analysis of Biological Characteristics among P0 Proteins from Different Brassica Yellows Virus Genotypes. *Biology* **2021**, *10*, 1076. [[CrossRef](#)] [[PubMed](#)]
52. Kang, S.-H.; Qu, F.; Morris, T.J. A spectrum of HRT-dependent hypersensitive responses elicited by the 52 amino acid N-terminus of turnip crinkle virus capsid protein and its mutants. *Virus Res.* **2015**, *200*, 30–34. [[CrossRef](#)] [[PubMed](#)]
53. Michaeli, S.; Clavel, M.; Lechner, E.; Viotti, C.; Wu, J.; Dubois, M.; Hacquard, T.; Derrien, B.; Izquierdo, E.; Lecorbeiller, M.; et al. The viral F-box protein P0 induces an ER-derived autophagy degradation pathway for the clearance of membrane-bound AGO1. *Proc. Natl. Acad. Sci. USA* **2019**, *116*, 22872–22883. [[CrossRef](#)] [[PubMed](#)]
54. Zhang, X.-F.; Sun, R.; Guo, Q.; Zhang, S.; Meulia, T.; Halfmann, R.; Li, D.; Qu, F. A self-perpetuating repressive state of a viral replication protein blocks superinfection by the same virus. *PLoS Pathog.* **2017**, *13*, e1006253. [[CrossRef](#)] [[PubMed](#)]
55. Kumar, T.K.S.; Samuel, D.; Jayaraman, G.; Srimathi, T.; Yu, C. The role of proline in the prevention of aggregation during protein folding in vitro. *IUBMB Life* **1998**, *46*, 509–517. [[CrossRef](#)]
56. Pemberton, T.A.; Still, B.R.; Christensen, E.M.; Singh, H.; Srivastava, D.; Tanner, J.J. Proline: Mother Nature’s cryoprotectant applied to protein crystallography. *Acta Crystallogr. Sect. D Struct. Biol.* **2012**, *68*, 1010–1018. [[CrossRef](#)] [[PubMed](#)]
57. Ramos-Sobrinho, R.; Adegbola, R.O.; Lawrence, K.; Schrimsher, D.W.; Isakeit, T.; Alabi, O.J.; Brown, J.K. Cotton Leafroll Dwarf Virus US Genomes Comprise Divergent Subpopulations and Harbor Extensive Variability. *Viruses* **2021**, *13*, 2230. [[CrossRef](#)]
58. Tabassum, A.; Bag, S.; Suassuna, N.D.; Conner, K.N.; Chee, P.; Kemerait, R.C.; Roberts, P. Genome analysis of cotton leafroll dwarf virus reveals variability in the silencing suppressor protein, genotypes and genomic recombinants in the USA. *PLoS ONE* **2021**, *16*, E0252523. [[CrossRef](#)]
59. Csorba, T.; Lózsa, R.; Hutvágner, G.; Burgyán, J. P0 protein of tobacco etch virus prevents the assembly of small RNA-containing RISC complexes and leads to degradation of ARGONAUTE1. *Plant J.* **2010**, *62*, 463–472. [[CrossRef](#)]
60. Li, S.; Le, B.; Ma, X.; Li, S.; You, C.; Yu, Y.; Zhang, B.; Liu, L.; Gao, L.; Shi, T.; et al. Biogenesis of phased siRNAs on membrane-bound polysomes in Arabidopsis. *eLife* **2016**, *5*, e22750. [[CrossRef](#)]

Disclaimer/Publisher’s Note: The statements, opinions and data contained in all publications are solely those of the individual author(s) and contributor(s) and not of MDPI and/or the editor(s). MDPI and/or the editor(s) disclaim responsibility for any injury to people or property resulting from any ideas, methods, instructions or products referred to in the content.